Plasma-surface interactions in atmospheric pressure plasmas: In situ measurements of electron heating in materials

S. G. Walton, B. M. Foley, J. Tomko, D. R. Boris, E. D. Gillman, S. C. Hernández, A. Giri, Tz. B. Petrova, and P. E. Hopkins

Citation: Journal of Applied Physics **124**, 043301 (2018); doi: 10.1063/1.5031821
View online: https://doi.org/10.1063/1.5031821
View Table of Contents: http://aip.scitation.org/toc/jap/124/4
Published by the American Institute of Physics

Plasma-surface interactions in atmospheric pressure plasmas: *In situ* measurements of electron heating in materials

S. G. Walton,[1,a)] B. M. Foley,[2,b)] J. Tomko,[3] D. R. Boris,[1] E. D. Gillman,[1] S. C. Hernández,[1] A. Giri,[2] Tz. B. Petrova,[1] and P. E. Hopkins[2,3,4]
[1]*Plasma Physics Division, Naval Research Laboratory, 4555 Overlook Ave. SW, Washington DC 20375-5346, USA*
[2]*Department of Mechanical and Aerospace Engineering, University of Virginia, Charlottesville, Virginia 22904, USA*
[3]*Department of Materials Science and Engineering, University of Virginia, Charlottesville, Virginia 22904, USA*
[4]*Department of Physics, University of Virginia, Charlottesville, Virginia 22904, USA*

(Received 31 March 2018; accepted 18 June 2018; published online 26 July 2018)

The energy flux to a surface during plasma exposure and the associated surface heating are of long standing interest as they contribute to the physico-chemical changes that occur during plasma-based materials synthesis and processing. Indeed, the energy delivered to the surface, via a flux of particles and photons, in concert with a flux of reactive species serves to chemically modify, etch, and/or deposit materials, with an efficacy that depends on the plasma processing environment. A unique feature of plasma synthesis and processing is that most of the delivered energy is absorbed at or very near the surface over short (picosecond) time scales. The dissipation of thermal energy proceeds through electron-electron and/or electron-phonon interactions as they propagate through the material, with relaxation time scales that can be orders of magnitude slower. Typically then, the surface is not in thermal equilibrium with the bulk material. Fast, surface-sensitive techniques are thus required to fully appreciate the dynamics of the plasma-surface interaction. In this work, we employ pump-probe Time-Domain Thermoreflectance, a surface sensitive technique typically used to measure thermal properties of thin films, to determine electron heating of thin metal films during exposure to an atmospheric pressure plasma jet. The results, in conjunction with current measurements, are used to develop a first order understanding of plasma jet-surface interactions. The results show that the energy delivered by the plasma jet causes a localized increase in electron energy within the thin film over an area commensurate with the plasma jet radius.
https://doi.org/10.1063/1.5031821

I. INTRODUCTION

One of the most important technological uses of non-equilibrium, low-temperature plasmas is in the synthesis and modification of materials. Low-pressure plasmas have long been used for applications ranging from surface functionalization to thin film growth and etching. More recently, there has been a growing effort to advance the use of atmospheric pressure plasmas in the processing and treatment of materials and systems, particularly those that are not compatible with low-pressure environments such as biological materials[1–3] and liquids.[4–6] Regardless of the operating conditions or applications, a well-recognized attribute that separates plasma-based approaches from other processing techniques is the synergistic effect associated with the simultaneous delivery of both chemically active species and energy to a material's surface.[7] The latter is an essential component in driving physical and chemical processes either directly through particle and photon interactions or indirectly via surface heating. It is not surprising then that a number of studies have been aimed at understanding and quantifying the energy flux to a surface immersed in a plasma and the resulting thermal load for both low pressure[8–10] and atmospheric pressure[11] plasma systems.

One can begin to understand the response of a material immersed in a plasma by considering the power balance at the surface[8] given by

$$P_{in} = P_{heat} + P_{out}. \quad (1)$$

Here, P_{in} is related to the energy flux (or power flux-density) into the material, P_{out} to the energy flux leaving the material, and P_{heat} is the power that heats the material. P_{in} is determined by accounting for all collisional and radiative sources of energy from the mix of charged particles (electrons and ions), reactive gas molecules and atoms, and excited species generated in the gas phase that impact the material surface or produce photons that reach the surface, as well as exothermic chemical and physical reactions at the material surface and system controls such as substrate heating and/or biasing. Similarly, P_{out} is determined by accounting for all the processes that remove energy from the surface including particles that leave the surface (or diffuse into the bulk), radiation, endothermic reactions, and system components that serve to cool the material. The difference between P_{in} and P_{out} is the power that heats the substrate, P_{heat}. While it

a)scott.walton@nrl.navy.mil
b)Current Address: George W. Woodruff School of Mechanical Engineering, Georgia Institute of Technology, Atlanta, Georgia 30332, USA

is a difficult task to properly account for all sources that contribute to P_{in} and P_{out} in even the simplest plasma processing environments, a quantifiable measure is accessible by monitoring the temperature of the materials exposed to the plasma. While of practical interest, it is important to note that temperature is a macroscopic property that describes the statistical distribution of particle energies within the material and thus, not a direct measure of the energy flux. To address this, devices and techniques have been developed[12–14] to measure the thermal flux directly by measuring the *change* in temperature over some distance or time.

Despite the advances in technology, measuring the energy flux to a surface remains challenging. To understand this, consider that most particle energy is delivered and adsorbed rapidly within a few nanometers of the surface. For example, Graves and Humbird[7] estimate that Ar^+ ions with 200 eV of kinetic energy release most of their energy within about 25 Å of the surface in about 10^{-12} s. Anders[15] argues that the potential (ionization) energy is released at (or very near) the point of contact during neutralization of ions and absorbed locally within the same time scale. This will also be true for other particles possessing kinetic energy (e.g., fast neutrals), potential energy (e.g., metastables), or both. Photons will typically penetrate much deeper than particles with low-energy, with IR range photons generally penetrating farther than high-energy, VUV range photons. However, when they do lose their energy, it is lost nearly instantaneously. The point being that the energy delivered by particles or photons produces a well-localized "thermal spike" that exceeds the average temperature of the material and rapidly dissipates. The reason for this is that energy transport in a solid is largely mediated by electrons and lattice vibrations or phonons, which are typically characterized by mean free paths on the order of several to hundreds of nanometers and relaxation times that range from several femtoseconds for electrons to picoseconds or even nanoseconds for phonons.[16] In other words, the time required to propagate energy away from a plasma-interaction zone near the surface, determined by the electron and phonon diffusion times, can be much longer than typical times associated with P_{in}. Thus, it would be of fundamental interest to study the behavior and resulting energy transport processes of the thermal energy carriers during plasma-surface interactions, which is the focus of this work.

To this end, we employ pump-probe Time-Domain Thermoreflectance (TDTR) as a temperature probe to measure the thermo-electric response of thin (80–200 nm) gold films subject to an atmospheric pressure plasma jet. The approach utilizes femtosecond laser pulses to rapidly heat (or "pump") a material, followed by a series of similarly fast but much lower power laser pulses that are delayed in time with respect to the pump to monitor (or "probe") the variation in temperature via the change in surface reflectivity of the probing laser. Pump-probe TDTR metrology is typically used to measure the thermal conductivity of bulk materials as well as thin layers with micron-scale resolution.[17,18]

While optical techniques have been utilized to monitor reflectivity,[14] the short time scales investigated during the TDTR measurements described here are compatible with the time scales associated with energy deposition during plasma exposure and can be used to monitor the propagation of thermal energy carried via electrons and phonons.

II. EXPERIMENTAL

For this work, an atmospheric plasma source was integrated into a time domain thermoreflectance (TDTR) system. TDTR is an optical pump-probe method for measuring energy transport and relaxation mechanisms within a wide variety of nano/micro material systems.[17,18] The technique uses pulsed lasers with femtosecond durations to both heat (pump) the material and sense (probe) the change in temperature. The pulses in the pump beam are amplitude-modulated using an electro-optical modulator at a user-defined frequency, and the wavelength of the beam is converted from 800 nm to 400 nm via a bismuth triborate (BiB_3O_6) crystal. An inline power meter is used to measure the time-average laser power delivered to the surface. The modulated pump beam results in a temperature oscillation at the sample surface, which will then affect the reflected probe beam due to changes in the thermoreflectance (dR/dT) of the material. The temperature changes induced in the sample by the pump are extremely small, requiring lock-in detection of the thermoreflectance changes encoded in the reflected probe beam. Prior to arriving at the sample, the probe beam is routed down a mechanical delay stage to elongate the beam path in adjustable increments. By varying the arrival time of the probe pulse relative to the pump pulse, the time-evolution of the sample surface temperature due to the heating event can be ascertained. The use of femtosecond pulse widths results in excellent temporal resolution, enabling the investigation of energy deposition and dissipation processes from picosecond to nanosecond time scales.

In the current TDTR experiments, the pump and probe laser pulse widths are roughly 600 and 200 fs, respectively, at the sample surface. The pump laser is amplitude modulated at a frequency of 11.39 MHz. Typical minimum temporal increments on the delay stage that enable the pump-probe time delay are much less than the probe pulse width ($<$10 fs), with a maximum possible time delay of about 7 ns. In this work, we focus on the time regime from pulse absorption up to a few picoseconds after pulse absorption. Upon absorption by a sub-picosecond pulse, the electrons in the metal are excited and consequently heated to temperatures much higher than the lattice temperature. Thermalization between the electron and phonon subsystems typically occurs on the order of 1–10 ps in metals, and its relaxation is based on both electronic and lattice temperatures.[19] During this electron-phonon nonequilibrium process, the highly energetic electron gas will cool with its surroundings and could be strongly influenced by any additional energy input or carrier (e.g., the plasma jet). Thus, this temporal regime during TDTR will provide a unique sensitivity to monitor the excited electron gas when a material is interacting with a plasma jet.

The atmospheric pressure plasma jet used for the experiment was constructed at the Naval Research Laboratory and based on coaxial, DBD designs.[20] Specifically, a small diameter, hollow metal tube carrying helium gas is located within

a ceramic tube (r = 0.8 mm) that extends out of the end of a grounded cylindrical metal casing. The metal tubing (powered electrode) is connected to a high-voltage source through an electrical feedthrough in the wall of the grounded metal casing. The end of the casing necks down to effectively form a ground ring near the end of the ceramic tube. A discharge is thus generated within the gas flow between the metal tube driven at high voltage and the ground ring at the end of the tube. A plasma plume emerges from the end of the ceramic tube and passes through the ambient before termination at adjacent surfaces. The gas concentration changes rapidly as the helium mixes with air. The jet can be driven by a variety of power supplies. In this work, both AC (36 kHz, Vpp = 1–3 kV) and pulsed DC (1–5 μs pulse width, 1%–10% duty factor, V = 2 kV) are employed. The carrier gas is He and typical gas flows are 5–10 l/min. Note that at these voltages, a plasma is only produced when the helium is flowing. High voltage probes (North Star High Voltage; Model # PVM-5) are used to measure the instantaneous applied voltage and current transformers (Pearson Electronics, Inc.; Model #4100) are used to measure the currents delivered to the driven electrode and surface in contact with the plasma plume.

In these experiments, the optically excited carrier dynamics within a thin gold film deposited by electron-beam evaporation on a fused quartz or silicon substrate was monitored using TDTR as the plasma jet operating parameters were varied to change the flux of species delivered to the Au surface, as well as the position with respect to the plasma jet point of contact (see Fig. 1 for schematics of the experiments). The thickness of the Au film was determined via profilometry (Bruker Dektak XT). The electrical resistivity of the Au film was measured via a four-point probe to be 2.926 $\times 10^{-6}$ Ω-cm, resulting in a calculated thermal conductivity of 246 W m^{-1} K^{-1} via the Wiedemann-Franz law. An electrical probe in contact with the Au thin film provides a path to ground for the plasma current. The plasma source voltage, source current, and surface current were all captured through oscilloscope (Lecroy Corp; Model # LC584AL) traces. The laser spots used for TDTR were focused onto the sample surface and easily fit within the area irradiated by the plasma jet. The $1/e^2$ radii of the pump and probe laser spots were 18 and 9 μm, respectively, and were determined using a ThorLabs scanning slit optical beam profiler. TDTR scans spanning delay times of −2 to 3 ps were collected with and without the plasma operating over a range of conditions. Note that a pump-probe time delay of t = 0 ps corresponds to the maximum TDTR signal after pulse absorption, roughly equivalent to the maximum electron temperature in the metal; thus, pulse absorption occurs before t = 0 ps using our nomenclature. The plasma source was mounted on a micrometer stage allowing the plasma jet point of contact to be varied with respect to the TDTR measurement.

III. RESULTS AND DISCUSSION

Plasma jets, like the one employed here, are typically produced in a noble gas flowing through a cylindrical DBD configuration using either AC or pulsed DC voltage waveforms and then allowed to expand into the ambient at the end of the tube.[20–22] The approach yields a plasma plume that extends from the exit of the tube. The plume, however, is not uniform but rather varies strongly in both time and space according to the applied voltage, driving frequency, and downstream gas mixing.[23,24] Thus, any interactions with surfaces will have similarly strong temporal dependencies. Figures 2 and 3 show the applied power and surface currents measured in this work. The AC jet (Fig. 2) employs a 36 kHz AC high voltage (Vpp ≤ 2 kV) signal. The "no jet" signals are acquired in the absence of a helium flow and represent the displacement currents within the circuit, which can be used to determine the plasma currents by subtracting them from the measured current when the plasma is operating. When the gas is turned on, indicated as "jet" in the plots, a small bump on the current trace at about 2 μs indicates the ignition of the plasma. Shortly after, a large increase in

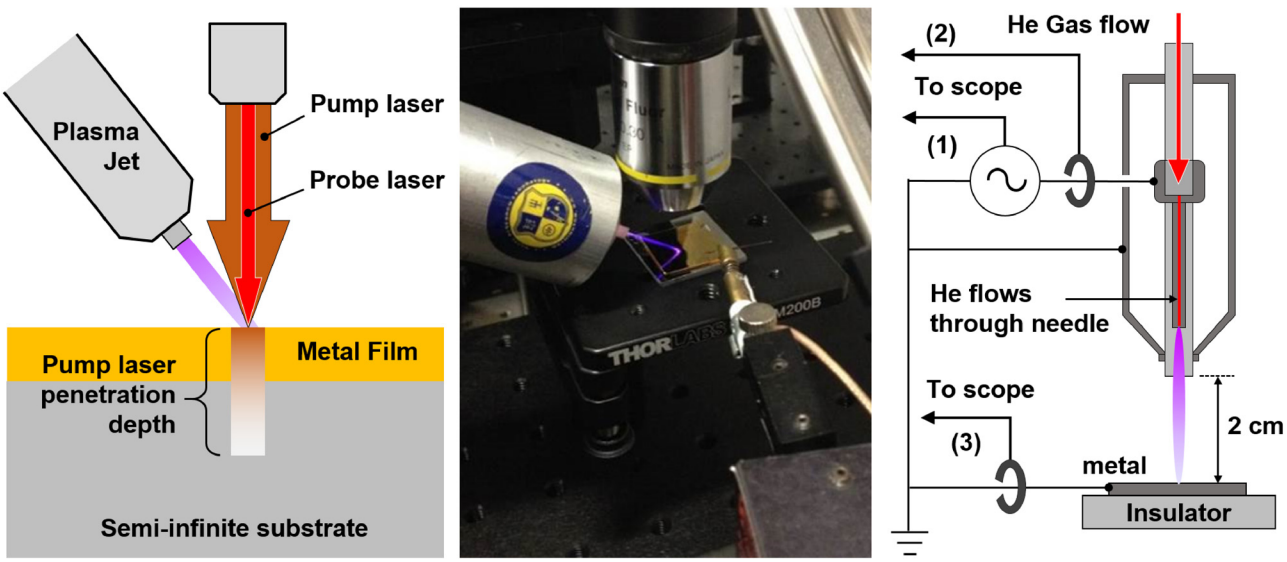

FIG. 1. The experimental layout. (Left) A schematic of the plasma jet, TDTR lasers, and surface along with (Center) an image of the setup. (Right) Plasma jet schematic showing the driving circuit and electrical diagnostics.

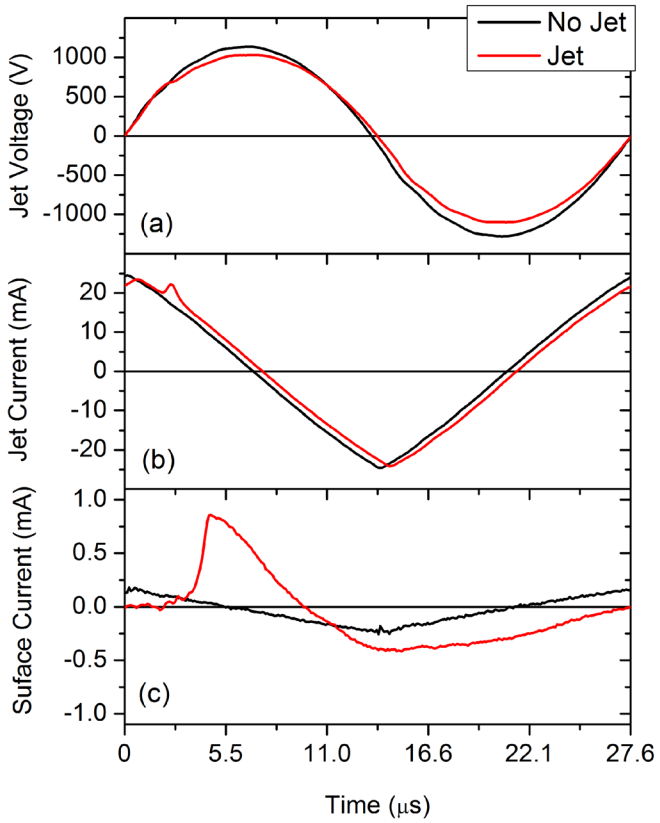

FIG. 2. Characteristic voltage and current traces of the plasma jet driven with 36 kHz AC signal. "No Jet" and "Jet" correspond to the voltage and current without and with gas flow, respectively. Without gas flow, a plasma jet plume is not visible. (a) The applied voltage and (b) measured current to the driven electrode. (c) The measured current at an electrode located downstream from the exit of the jet. The results in a, b, and c are measured at locations 1, 2, and 3, respectively, in Fig. 1(c).

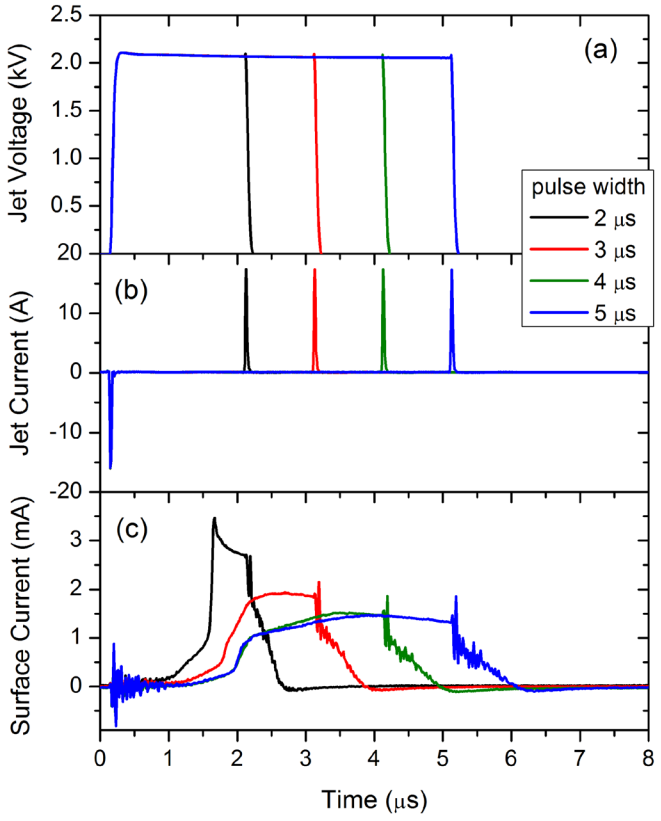

FIG. 3. Characteristic voltage and current traces of the plasma jet driven with pulsed DC at a 2%–5% duty factor. (a) The applied voltage and (b) measured current to the driven electrode. (c) The measured current at an electrode located downstream from the exit of the jet. The results in a, b, and c are measured at locations 1, 2, and 3, respectively, in Fig. 1(c).

surface current is observed as the plasma "collides" with the surface. Although there is no strong indication of plasma generation at the electrode on the negative swing of the applied voltage, a noticeable increase in surface current is observed. We correlate these observations with a plasma-surface interaction dominated by ions during the first half of the period and by electrons and negative ions during the second half. In contrast, the jet driven by pulsed DC (2–5 μs; 2%–10% duty factor) utilizes a positive high voltage and so the flux to the surface is dominated by positive ions (see Fig. 3). For the surface currents in Fig. 3(c), we have already subtracted off the displacement currents. Note that the large current spikes at the beginning and end of the pulses [Fig. 3(b)] are predominantly associated with rapidly raising and lowering the potential of the electrode. The resulting fields also drive short oscillations in the surface current at turn on/off. Regardless of the approach, the results clearly show that the plasma-interface should be considered a dynamic environment, which varies strongly in time.

The initial results showing the thermoreflectance response of 200 nm gold films on silicon substrates subject to an atmospheric pressure plasma jet driven in the AC mode are shown in Fig. 4. For these measurements, the TDTR lasers are co-aligned with the plasma jet point of contact at the surface. Figure 4(a) shows the TDTR signals as a function of pump-probe delay time acquired with and without the jet operating. Both data sets follow a general trend expected for TDTR measurements. That is to say, the pump laser excites the materials while the probing laser tracks the thermal excitation and subsequent cooling. When the jet is present however, the signal intensity is generally greater. Normalizing the signals to the peak intensity, as shown in Fig. 4(b), also indicates a difference in cooling profiles. Figure 4(c) shows a "stare" mode measurement, where the peak in the TDTR signal [from Fig. 4(a)] is tracked in laboratory (real) time as the plasma is turned on and off. The increase in absolute intensity when the plasma is turned on suggests a higher surface temperature when the plasma is on.

The results indicate plasma heating of the surface; however, it is important to note that the systems are not synchronized in time because the present configuration does not allow for a way to appropriately gate and/or trigger either the plasma jet or the pump laser. Thus, the TDTR results are a measurement of the time-averaged heating by the jet. While the plasma-surface interface is certainly dynamic, other experimental factors such as the influence of electric fields generated by the jet driving circuit may influence the results. To address this, the experiment was reconfigured by eliminating the pump laser and instead locking-in to the heating fluctuations in the metal film at the plasma driving frequency that are detected by the reflectivity of the probe laser. The improvement in sensitivity provided by this configuration enabled us to evaluate both the transient temporal

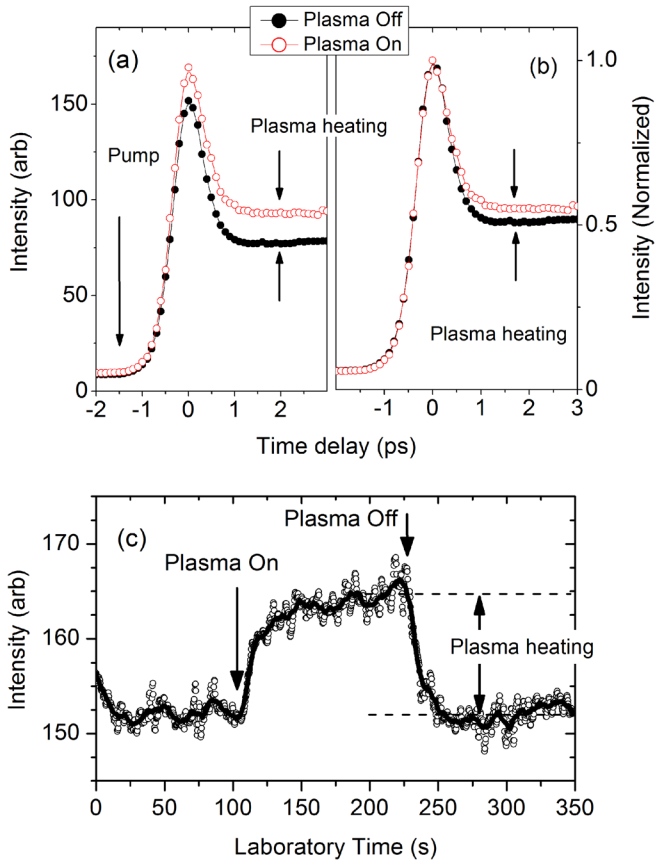

FIG. 4. TDTR measurements showing the effect of the plasma jet. (a) TDTR signal intensity as a function of pump-probe delay time with and without the plasma jet operating and (b) those signals after normalizing to the peak intensity. The latter illustrates the differences in signals after accounting for any experimental variations. (c) The peak TDTR signal with and without plasma running as a function of lab time (real time). The solid line is the raw data (open symbols) after smoothing. The measurements employ an AC-driven jet and the material is 200 nm thick Au films on Si substrates. The laser and jet spots at the surface are co-aligned.

response of the plasma-surface interaction on the time scale of seconds as the power and gas supplied to the plasma jet are turned on and off and the spatial profile of the plasma jet interaction at the surface of the metal film. Shown in Figs. 5 and 6 are the time-dependent results of those measurements. The measurements are analogous to the measurements in Fig. 4(b) except that the driving voltage waveform of the plasma jet replaces the pump laser as the primary heating frequency. For the remainder of this paper, we report results for 80 nm Au films deposited on quartz substrates.

Figure 5 shows the time profile using the AC jet (36 kHz) with probing laser signal phase-locked to 36 kHz. The signal increases strongly as the jet is turned on at t = 0 s and remains nearly constant until the gas flow is turned off at ≈27 s. Between then and ≈60 s, the AC power remains on. The absence of gas flow ensures that no plasma jet is produced and so, the non-zero signal indicates an effect due to the AC power. To understand this better, the experiments were repeated using pulse DC rather than AC. The results in Fig. 6 show the time profile using a plasma jet driven with a 4 μs long, 2 kV pulse running at 10 kHz. Unlike the AC results, the signal goes to zero when the gas flow is turned off but applied power remains on. While the reasons for this

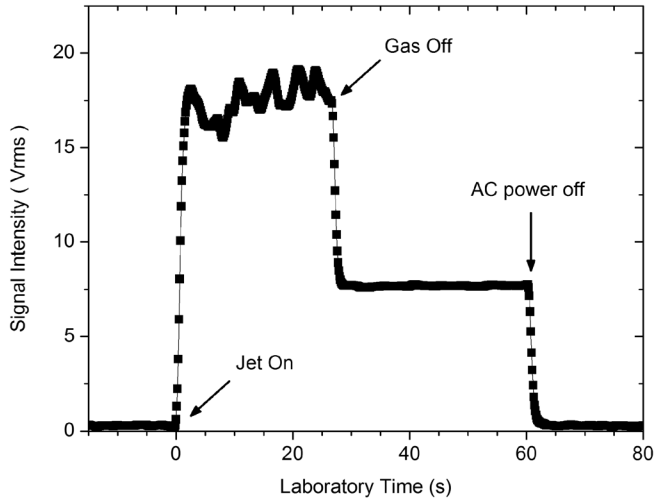

FIG. 5. The change in thermoreflectance produced by the AC plasma jet impacting an 80 nm Au film on a quartz substrate. Shown is the probe laser response, phase-locked to the plasma driving frequency (36 kHz), as a function of time. When the plasma jet is turned on ("Jet on"), the gas is flowing and power is on. Between "Gas off" (≈ 27 s) and "AC power off" (≈ 60 s), the gas flow is turned off but power remains on. During this mode, there is no visible plasma plume. Note that the signal does not go to zero when the gas flow is off.

difference are not known, we speculate AC fields drive inductive heating in the gold film. Importantly, the measurements of Figs. 5 and 6 suggest a correlation between the plasma jet operation and changes in the surface reflectivity produced by elevated temperatures in the film. It is important to note that with either jet, the reflectance signals before and after jet irradiation are identical, indicating that the plasma does not affect the surface in ways that would change the reflectance.

To further explore this correlation, measurements to probe the spatial extent of this heating were performed. The

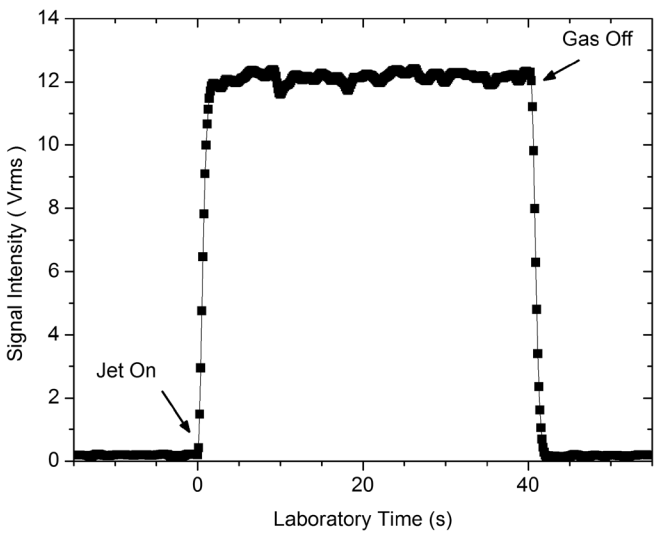

FIG. 6. The change in thermoreflectance prompted by a pulsed plasma jet (pulse width = 4 μs; period = 100 μs). Shown is the probe laser response, phase-locked to the plasma driving frequency (10 kHz), as a function of time. When the plasma jet is turned on ("Jet on"), the gas is flowing and power is on. At ≈27 s ("gas off"), the gas flow is turned off but power remains on and no plasma plume is visible. In contrast to the AC plasma jet, the signal does go to zero when the gas flow is turned off.

results are shown in Fig. 7, where the plasma jet point of contact on the surface is varied with respect to the laser spot. In this case, the jet is driven with pulsed DC (4 μs; 10 kHz). Figure 7(a) shows the signal intensity acquired while moving the plasma jet through the laser point of contact where 1 s corresponds to approximately 2 μm. This suggests a heating zone with a diameter of about 0.5 mm, which is about 1/3 the inner diameter of the tube from which the jet emerges. Figure 7(b) shows the same measurement while moving in the opposite direction. The slight asymmetry in the signal intensity in both figures is consistent and likely due to the measurement geometry (e.g., the jet is incident to the surface at an angle). Nonetheless, the data support the aforementioned correlation between the plasma jet and surface heating.

Figure 8 compares the signal response for a jet driven with pulsed DC at 10 kHz for 4 μs and 8 μs. An increase in signal intensity is seen for a longer pulse duration (note that the scale difference between the left and right ordinate is a factor of 2), which is correlated with a relative increase in temperature within the material. A somewhat broader distribution is also seen for the longer pulse duration, suggesting that a longer plasma exposure drives a larger thermal response that is dissipated over a larger area.

Taken together, the results of Figs. 5–8 strongly suggest the observed elevation in TDTR peak intensity [Fig. 4(b)] and changes in TDTR profiles [Fig. 4(a)] are, in fact, caused by the plasma jet interactions with the surface. The TDTR measurements, on the other hand, can be related to the energy of the electrons and their collision dynamics. As such, the TDTR technique provides a method to examine plasma-driven surface interactions that elevate the energy of electrons within the metal.

Accordingly, we revisit the TDTR measurements shown in Fig. 4 using plasma jets driven by both AC and pulsed DC. Figure 9 shows the results for the AC Jet (36 kHz) generated at different applied voltage amplitudes (the values

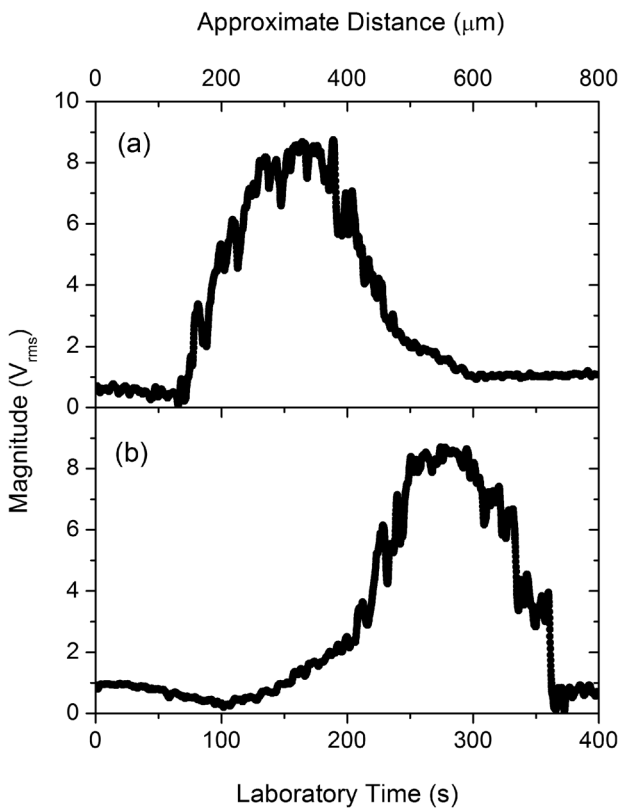

FIG. 7. The change in thermoreflectance produced by a pulsed plasma jet (pulse width = 4 μs; period = 100 μs) as a function of distance from the plasma plume point of contact on the surface. (a) Signals acquired while moving the plasma plume through the laser center point of contact where 1 s corresponds to approximately 2 μm. (b) The same measurement while moving in the opposite direction. The slight asymmetry in the effective heating region is likely due to the experimental configuration.

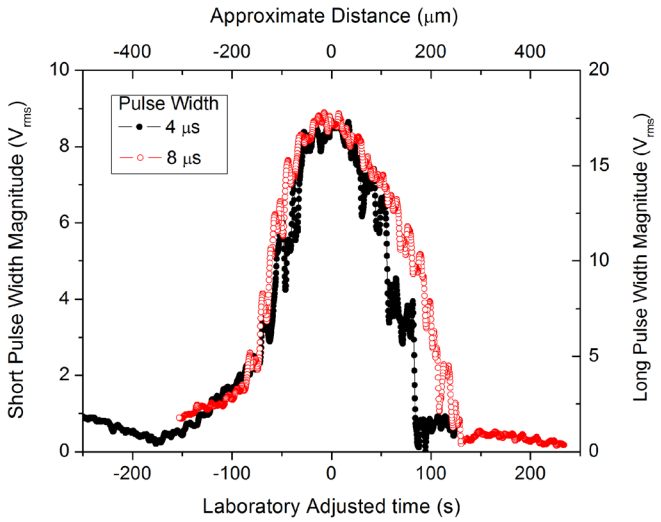

FIG. 8. The change in plasma-driven thermoreflectance as a function of position for pulsed (10 kHz) jets with pulsed widths of 4 μs and 8 μs. The left ordinate corresponds to the signal intensity of the probe laser response when the pulse width is 4 μs, while the right corresponds to the signal intensity when the pulse width is 8 μs. Note the factor of 2 difference in intensity along with a slightly broader profile when the pulse width is 8 μs.

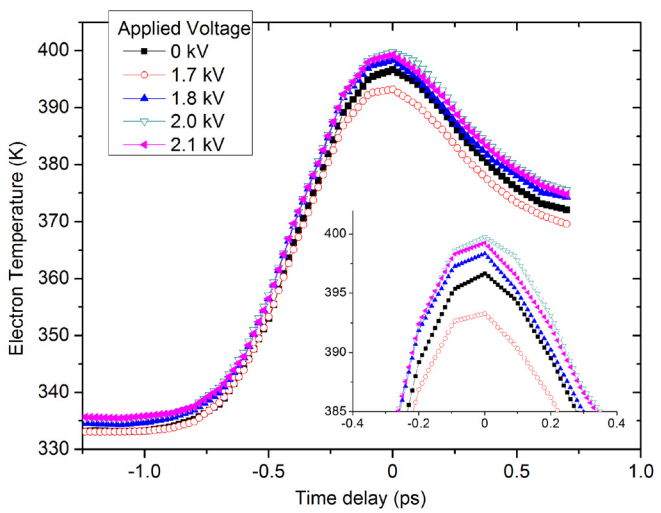

FIG. 9. TDTR measurements with electron energy fitting using an AC jet (36 kHz) driven at different applied voltage amplitudes. The values for applied voltage are peak-to-peak voltage. Also shown is the baseline case when the jet is not operating (0 kV). The inset shows an expanded view of the data at t = 0 (or peak intensity). The measurements indicate an increase in the time-average electron energy (temperature) within the material is expected when the applied voltage is increased.

reported are peak-to-peak voltages). Figure 10 shows a pulsed DC (10 kHz) jet driven using different pulse widths (i.e., the duty factor is varied). For these datasets, the time-dependent response was fitted using the procedure described in Refs. 25 and 26 to determine the electron temperature within the material. Again, it is important to note that the TDTR measurements and the operation of the plasma jets are not synchronized in time. Thus, the TDTR measurements and the derived electron temperatures should be considered the time-averaged response to both the plasma jet and the pump laser. For example, the fact that the baseline energy is above that expected for materials at room temperature (≈293 K) is largely determined by the time-averaged heating of the pump laser (or thermal accumulation), which is operated at a much higher frequency than the plasma jet.[27,28] For comparison, we include TDTR measurements without the plasma running and when only gas was flowing in Fig. 10.

The relevant metric to consider for the plasma heating is the difference in TDTR signal intensities and derived energies as the driving voltage and pulse width of the jet are varied. With two notable exceptions, the measurements indicate an increase in both the baseline and peak electron temperature (or energy) when increasing the applied voltage in the case of an AC jet and when increasing the length of time the voltage is applied in the case of a pulsed DC jet. The exceptions to this trend are for the lowest voltage amplitude (1.7 kV) and the shortest pulse width (2 μs) measured, where the peak temperatures are observed to be lower than the case of no plasma jet. It is reasonable to expect some cooling associated with the gas flow impinging the surface due to increased convection coefficients. However, no discernible difference is observed between the TDTR results when gas is flowing ("gas on") and not ("gas off") shown in Fig. 10. Nonetheless, we conclude that an increase in electron energy within the material follows from an increasing driving power in the AC jets and for longer plasma exposures in the pulsed jets. For cases where power is low and or duration is short, we speculate that perhaps a plasma-stimulated cooling mechanism exists. Additional studies are required to fully understand this.

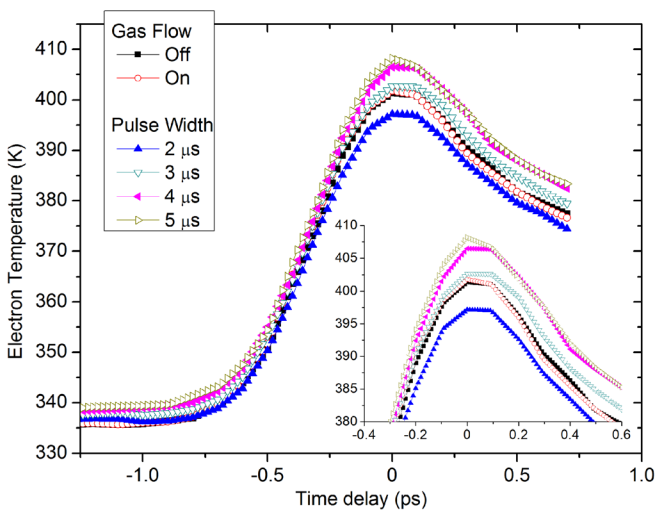

FIG. 10. TDTR measurements with electron energy fitting using a pulsed (10 kHz) jet driven at different pulse widths. Also shown are the baseline cases when the jet is off ("Gas off") and when only the gas is flowing ("Gas on"). The inset shows an expanded view of the data at t = 0 (or peak intensity). The measurements indicate an increase in the time-average electron energy (temperature) in the material is expected when longer voltage pulses are applied.

To clarify the relationship between the measurements and the surface temperature, there are two timescales to consider. The surface temperature can be considered a long term response—when the electrons are in thermal equilibrium with the lattice—and is related to the rise (or fall) of the baseline level of the TDTR profiles when compared to the TDTR profiles when the jet is not running. The baselines increase by up to a few degrees Kelvin during plasma exposure, which is supported by simple IR imaging (not shown) that indicates a similar increase in temperature. The second timescale involves the adsorption and dissipation of the pump laser energy, which is short (picoseconds). Because the pump laser power is constant, the plasma-induced increase (or decrease) in peak intensity also indicates a difference in electron energies during plasma irradiation. The difference in cooling profiles (as noted in Fig. 4) also suggests changes in kinetics, but is not the focus of this work.

The temperature increase resulting from plasma exposure shown in Figs. 9 and 10 is small (≤10 K) but, as we will argue, reasonable. To begin, we can use the V-I characteristics of the plasma jets to determine the power absorbed by the plasma and estimate the energy flux (or power flux-density) at the surface. For the AC jet, it is straightforward to determine the power delivered to the plasma jet using the measured voltage and current profiles shown in Figs. 2(a) and 2(b). Figure 11(a) shows the instantaneous power delivered to the electrode over one period for a range of applied voltages. The average of each is the power per period and always positive. Figure 11(b) shows the corresponding net surface currents (displacement currents have been accounted for). While the magnitudes of the positive and negative currents vary with applied voltage, the average surface current over one period is always found to be zero. It is worth noting that for voltages below about 1.6 kV, the jet does not appear (visually) to be in contact with the surface. Above 1.6 kV, it is and that observation corresponds to a notable increase in surface currents. From 1.8 to 2.1 kV, the surface currents exhibit a temporal shift, but are otherwise comparable.

The power adsorbed by the plasma jet during one period is the difference between the average power when gas is flowing and when no gas is flowing (recall the jet is only produced at these voltage levels when a noble gas is present). Figure 12 shows the power absorbed by the plasma during one period as a function of applied voltage and is found to be approximately linear with applied voltage. As illustrated in Fig. 12, the net surface currents do not appear to follow the same linear behavior and so it is reasonable to assume that only a fraction of the power adsorbed by the plasma is transferred to the surface.

The measured surface currents [Fig. 11(b)] can be employed to estimate the energy flux, P_i, supplied by charged particles to the surface using

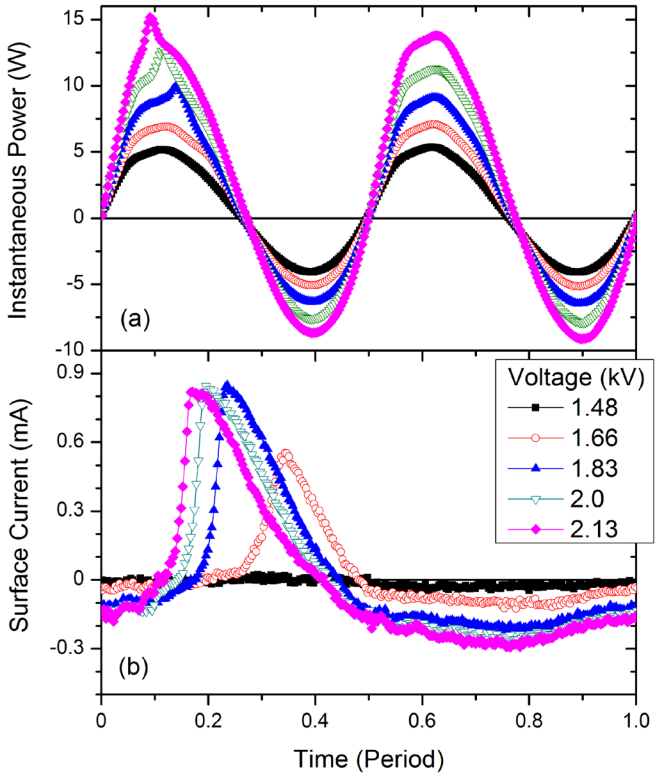

FIG. 11. Power and current measurements during one period of an AC plasma jet (36 kHz) operating at different applied voltages. The values for applied voltage are peak-to-peak voltage. (a) The power applied to the electrode. (b) The net current delivered to a surface located about 2 cm from the exit of the plasma jet source.

$$P_i = \Gamma_i E_i = I_i E_i / A, \tag{2}$$

where Γ_i is the fluence of species i, E_i is its energy, I_i is the corresponding measured current, and A is the area irradiated by the plasma jet. The particle composition and energies at the surface in this work are not known. However, it is reasonable to assume that the kinetic energy of the charged particles incident on the surface is modest. Measuring the energy of ions incident on a surface in atmospheric pressure plasmas is a challenge[29] and so, the available data are limited. Still, measurements[30–32] and simulations[33] suggest that the kinetic energy of the positive ions supplied by low power, atmospheric pressure plasma is likely to be less than 5 eV and only a fraction of that will be transferred to the surface.[34] Positive ions can also transfer a fraction of their potential energy, in an amount equal to the difference between the ionization potential and the surface work function. Because of the standoff distances used and the rapid mixing of helium with air,[23,24] we assume that the dominant ions at the surface are O_2^+ and N_2^+ rather than He^+, because of the lower ionization thresholds of O_2 (IE =12.1 eV) and N_2 (IE =15.6 eV) compared to He (IE =24.6 eV). The energy transferred to the gold substrate ($\varphi \approx 4.5$ eV) is then in the range of about 7–11 eV. The expected kinetic energy of electrons at the surface is even less known. The energies in bulk vary according to the discharge type and operating conditions over a range of 1–10 eV, or higher.[24,33] A substantial amount of negative ions are also produced in atmospheric pressure plasmas and likely contribute to the measured negative current at the substrate.[23] However, for the AC jet used in this work, it is fair to assume that for a majority of the time, the kinetic energy of all species at the surface is likely to be a fraction of an eV—perhaps even thermal—given their respective mean free paths at atmospheric pressure are much shorter than the expected sheath thickness.

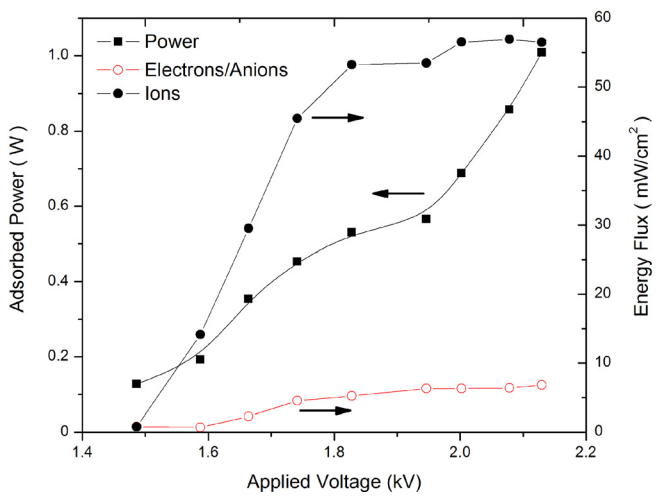

FIG. 12. Power adsorbed by the plasma and estimated energy flux to the surface over one period of AC plasma jet operation as a function of applied voltage (given as peak-to-peak voltage). The values for adsorbed power are determined by the difference between the applied power when the jet is on [Fig. 11(a)] and the applied power when the gas is turned off (not shown). The energy flux for ions and electrons is derived from the current measurements [Fig. 11(b)] using an ion energy of 10 eV and a negative ion and electron energy of 1 eV. Both the adsorbed power and energy flux increase as applied voltage increases.

Taking these considerations together, we adopt a time-averaged positive ion energy of 10 eV and a time-averaged energy for the electrons and negative ions of 1 eV. The difference in energies is due to the potential energy of the positive ions. We then use Eq. (2) to estimate the time-averaged energy flux of the positive ions by multiplying the average positive current (for one period) by the assumed energy of 10 eV and dividing by the area of irradiation, which is simply taken to be the cross-sectional area of the tube from which the jet emerges. For the electrons and negative ions, we follow the same procedure, using the average negative current and an energy of 1 eV. The results are shown in Fig. 12 as a function of applied voltage and suggest a total, time-averaged energy flux that ranges from about 20 mW/cm^2 at low power to about 70 mW/cm^2 at high power.

In the case of the pulsed DC jet, determining the power delivered to the plasma is less straightforward since most of the applied power goes into rapidly raising the voltage of the driving electrode. However, it is possible to estimate energy flux to the surface via charged particles using the current measured at the exposed surface from Fig. 3(c) as described above. The time-averaged current for one period is shown in Fig. 13 along with the estimated energy flux. Here, we have used the same positive ion energy values from above (10 eV) and irradiation area. The energy flux is found to increase with increasing pulse width, with values that are generally lower than but comparable to the estimated values for the AC jet.

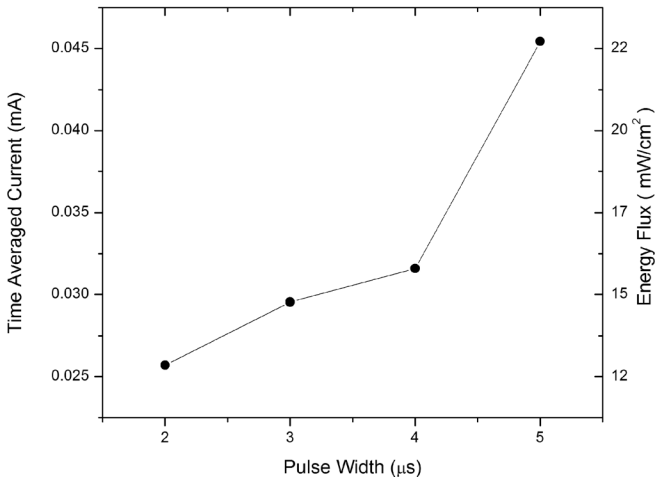

FIG. 13. The time-averaged current and corresponding ion energy flux over one period for a pulsed jet (10 kHz) as function of pulse width. The results are derived from the surface current measurements in Fig. 3 and the estimated energy flux assumes an ion energy of 10 eV.

The temperature response of thermal probes and the derived energy flux subjected to an RF (1.7 MHz) driven plasma jet have been previously reported.[11,35] In these works, the jet was produced in a flow of argon at a power 65 W and the thermal probe was located at various distances downstream from the jet. Generally, those measurements determined that the energy flux to the surface on the order of hundreds of mW/cm^2 produced surface temperatures of as much as 55 °C (about 30 °C above room temperature). In other words, the power delivered to the plasma and energy flux to the surface were over an order of magnitude higher than those observed in the present work and resulted in a significantly larger rise in surface temperature. The energy flux from high power (∼1–4 kW) plasma jets has also been measured.[36,37] In those systems, the energy flux is ∼100–300 W/cm^2, producing temperature increases of up to 400 °C. Of course, the measured surface temperature via thermal probes is not the same as the electron temperatures measured via TDTR but, they are related and so, we conclude the small electron temperatures measured in our work are reasonable.

To better benchmark the measurements here, it is possible to vary the pump laser power to reproduce the electron energies shown in Figs. 9 and 10. Specifically, we observed that an increase in time-averaged laser power from 30 mW to 33 mW (averaged power as measured by the power meter) was sufficient to produce a TDTR response comparable to when the plasma was operating. Using the pump laser spot size (r = 18 μm), the time-averaged energy flux at the surface increases from 2.947 kW/cm^2 to 3.242 kW/cm^2, or an increase in about 300 W/cm^2. That is to say, an energy flux of about 300 W/cm^2 was required to elevate the measured electron temperature in the material by about 10 K.

Upon first glance, the energy flux delivered to the surface (≈300 W/cm^2) by the laser needed to raise the electron temperature in the material does not compare favorably to the estimated energy flux from the charged particles (∼10 mW/cm^2) delivered by the plasma jet. However, it is important to note the vastly different spot sizes over which the pump heating and plasma heating are delivered. The radius of the plasma spot interacting with the surface is 800 μm, 44 times larger than the pump laser radius of 18 μm. The probe laser, which is monitoring the temperature rise, has a radius of 9 μm. Thus, while the pump and probe are of the same order during the TDTR experiment, the probe is only sampling a small fraction of the area of the sample heated by the plasma jet. This is reinforced by our previous discussion with respect to Figs. 7 and 8, where the change in reflectivity can be mapped across the plasma spot on the sample surface. Assuming that the energy delivered by the plasma jet is in the form of a Gaussian distribution across the plasma spot,[37] the region sampled by the TDTR probe beam with a 9 μm radius only measures the energy flux in the center portion of the Gaussian distribution of the jet. Thus, this energy flux sampled by the TDTR probe beam is drastically different than that calculated assuming the power is distributed uniformly across the 800 μm plasma jet spot. In other words, the energy flux from the plasma jet causing the change in the TDTR signal is *not* ∼10 mW/cm^2.

To rectify this, consider the plasma jet with a 10 mW/cm^2 energy flux distributed across a Gaussian distribution with a 1/e^2 radius of 800 μm. For a Gaussian beam, the 1/e^2 radius represents the radius in which the intensity drops to 1/e^2 of its axial, or peak value. When only considering a sampling of an inner radius of 9 μm outward from the center of this 800 μm Gaussian distribution, only the 9/800 (≈1%) inner most radius of the Gaussian is sampled by the probe beam. This will lead to a drastically different energy flux sampled by the probe since the intensity of a Gaussian distribution is not a linear function of radius. One-half of the power is contained within 59% of the 1/e^2 radius, and only about 10% of the power is contained within 23% of the 1/e^2 radius. The estimated energy flux shown in Figs. 12 and 13 for the plasma jet was calculated by assuming that the power is contained in an area ranging from radius $r = 0$ to $r(1/e^2) = \omega_0$ (i.e., we calculated the energy flux using the 1/e^2 radius of the plasma jet). Thus, the deposited power of the plasma jet with $\omega_0 = 800\ \mu$m is given by

$$P = P_o \int_0^{800\,\mu m} \left[\exp\left[\frac{-2r^2}{\omega_0^2}\right]\right] dr = 0.010\ \frac{W}{cm^2}\ \pi\omega_0^2 = 0.20\,\text{mW}, \tag{3}$$

where P_o is the peak power. Therefore, the fraction of power contained in the 9 μm radius sampled by the probe laser is given by

$$\frac{\int_0^{9\,\mu m} \exp\left[\frac{-2r^2}{\omega_0^2}\right] dr}{\int_0^{800\,\mu m} \exp\left[\frac{-2r^2}{\omega_0^2}\right] dr} = 0.0188. \tag{4}$$

Consequently, the power contained in this 9 μm inner radius of the 800 μm Gaussian plasma jet is 0.0188

(0.20 mW) = 3.78 μW. Hence, the plasma jet energy flux measured by the TDTR probe beam is $3.78 \times 10^{-6}/(\pi(9\,\mu\text{m})^2) \approx 1.5\,\text{W/cm}^2$.

Despite the relative similarity in pump and probe laser radii, the same methodology should be applied to determine the pump laser energy flux sample by the probe laser. Those results suggest that an energy flux of about $1.2\,\text{kW/cm}^2$ is required by the pump laser to reproduce the plasma-induced change in electron temperature within the material. Still, there remains a roughly three orders of magnitude discrepancy between this value and the equivalent plasma delivered energy flux ($1.5\,\text{W/cm}^2$).

However, it is important to recognize that lasers and plasmas, particularly the ones used here, will have very different energy deposition profiles as a function of depth and so, the stark difference in power deposition at the surface can be better understood by considering the volumetric power deposition of the TDTR pump laser and that of the plasma jet. The energy delivered by low energy charged particles is adsorbed at or very near the surface, while only a fraction of laser power is deposited in the film.[38] If we assume that the plasma energy deposition is limited to the top nanometer of the film, we arrive at a volumetric power deposition of roughly $1.5 \times 10^7\,\text{W/cm}^3$. For an opaque 80 nm Au film, the laser absorption scales as one minus the reflectivity at the pump wavelength (400 nm), suggesting that ≈60% of the pump light is adsorbed in the gold film. Moreover, the Au film thickness is less than the ballistic penetration depth of electrons in Au,[39] and therefore reasonable to assume that the energy penetration depth after laser heating is equal to the film thickness so that the adsorbed power is distributed along a column determined by the laser spot size and the film thickness. Thus, we arrive at a volumetric power deposition from the TDTR pump beam, as measured by the probe laser, of about $8.8 \times 10^7\,\text{W/cm}^3$, in general agreement with the volumetric power deposition of the plasma jet sampled by the TDTR probe, $\approx 1.5 \times 10^7\,\text{W/cm}^3$. In fact, if the assumed values of $\approx 10\,\text{mW/cm}^2$ were increased by a factor of 2–6 to better align with the highest values shown in Figs. 12 and 13, the agreement would be even better.

The agreement between the estimated energy deposition by the plasma and pump laser suggests that charged particles are, in this system, responsible for a fraction—perhaps substantial—of the observed heating. These, of course, are not the only species that deposit energy at the surface. Photons, energetic neutrals, and chemical reactions will all contribute to the energy flux.[8] Although it is not possible to discern the importance of these species from the present experiments, it is worth noting that the contributions from UV photons and chemical reactions are probably minimal in the present work. Indeed, the range of UV photons in full density air is short, suggesting that only those generated near the surface will be important. In addition, gold does not react with air or water and so exothermic surface reactions are likely not a significant contributor. Nonetheless, the flux of photons and reactive species at the surface will also increase with increasing charged particle fluxes and should be considered as part of the overall energy flux. It is not likely that the additional energy flux would significantly change the results above.

Broadly then, the reflectometry results (Figs. 5–8) show that the energy delivered by the plasma jet causes a spatially localized thermal spike at the point of contact, which dissipates radially. The TDTR results of Figs. 9 and 10 indicate that these results are related to the electron temperature within the material, suggesting a more detailed explanation. Specifically, the energy delivered via the flux of particles and photons causes the kinetic energy of the electrons within the material to increase over an area commensurate with the plasma jet radius. The mechanisms by which the energy is transferred remain unclear, but depend on which plasma species is carrying the energy. The kinetic energy of the heavy particles, for example, will likely be adsorbed by the lattice and then transferred to the electrons through electron-phonon interactions. In contrast, the energy of plasma electrons, UV photons, and metastable neutral species can be more directly transferred to the electrons. Regardless, the energy of the heated electrons will be dissipated through electron-electron collisions and electron-phonon interactions as they propagate radially from the point of contact. Although the measurements were time-averaged, the fact that the plasma oscillates in time implies that the magnitude of the heating has a temporal component as well.

IV. SUMMARY

In this work, we described a novel application of pump-probe Time-Domain Thermoreflectance (TDTR) to understand the thermo-electric response of surfaces exposed to atmospheric pressure plasma jets. TDTR employs a fast (<ps) laser pulse to rapidly heat a material, followed by a series of similarly fast (<ps) laser pulses to monitor the rise and fall in temperature via the change in surface reflectivity of the probing laser. The plasma jet was produced using both AC and pulsed DC waveforms to drive an electrode in a helium gas flow. The target surface in this work was a thin (∼100 nm) gold film on a quartz substrate.

To ensure that the material response was due to the plasma interacting with the surface, a series of measurements were performed using only the "probing" laser to show that reflectivity changes in the surface were correlated with the presence of the plasma. Specifically, the reflectivity of the surface was shown to change significantly when the plasma was turned on and off. Moreover, the maximum change in reflectivity was found to occur when the plasma jet and "probe" laser points of contact on the surface were co-aligned. The change in reflectivity was found to decrease as the laser spot was moved with respect to the plasma jet point of contact.

TDTR was then used to measure the heating of electrons within the material as the jet interacted with the gold film. The temperature of the electrons was found to increase as the intensity and duration of plasma irradiation were increased. Over the parameters studied, the temperature rise was less than 10 K. While modest, a combination of measurements and simple estimates suggests that the magnitude is reasonable for the conditions used in this work. It was also shown

that the flux of charged particles at the surface is likely to play an important role in the energy delivery to the surface.

The results of this work are in general agreement with previous works that measure temperature changes in plasma-exposed materials. This is to be expected given the manner in which the measurements were performed. Because the TDTR measurements and operation of the plasma jet are not synchronized in time, the measured increase in electron energies can be considered a time-averaged response to plasma irradiation. Conventional methods to measure temperature are similar in this regard. However, the TDTR measurements confirm that the energy flux leads to an increase in the kinetic energies of the electrons, which are the primary thermal energy carriers in metals, and thus provide valuable information about the adsorption and dissipation of the delivered energy. The prospects of doing time-resolved TDTR measurements using femtosecond lasers with picosecond resolution and micron-scale spot sizes are quite intriguing. In principle, such measurements could provide the ability to interrogate energy deposition and dissipation with fine spatial resolution over time scales associated with fundamental particle-surface interactions.

ACKNOWLEDGMENTS

This work was partially supported by the Naval Research Laboratory base program and the Office of Naval Research, Grant No. N00014–15-1–2769. This material is based upon work supported by the Air Force Office of Scientific Research under award number FA9550-18-1-0352.

[1]G. Y. Park, S. J. Park, M. Y. Choi, I. G. Koo, J. H. Byun, J. W. Hong, J. Y. Sim, G. J. Collins, and J. K. Lee, "Atmospheric-pressure plasma sources for biomedical applications," Plasma Sources Sci. Technol. **21**, 043001–043021 (2012).
[2]T. vonWoedtke, H.-R. Metelmann, and K.-D. Weltmann, "Clinical plasma medicine: State and perspectives of *in vivo* application of cold atmospheric plasma," Contrib. Plasma Phys. **54**(2), 104–117 (2014).
[3]M. Laroussi, "Low temperature plasma-based sterilization: Overview and State-of-the-Art," Plasma Process. Polym. **2**, 391–400 (2005).
[4]P. Bruggeman and C. Leys, "Non-thermal plasmas in and in contact with liquids," J. Phys. D: Appl. Phys. **42**, 053001–053028 (2009).
[5]D. Mariotti and R. M. Sankaran, "Microplasmas for nanomaterials synthesis," J. Phys. D: Appl. Phys. **43**, 323001 (2010).
[6]T. Kaneko, K. Baba, and R. Hatakeyama, "Gas–liquid interfacial plasmas: Basic properties and applications to nanomaterial synthesis," Plasma Phys. Controlled Fusion **51**, 124011–124018 (2009).
[7]D. B. Graves and D. Humbird, "Surface chemistry associated with plasma etching processes," Appl. Surf. Sci. **192**, 72–87 (2002).
[8]H. Kersten, H. Deutsch, H. Steffen, G. M. W. Kroesen, and R. Hippler, "The energy balance at substrate surfaces during plasma processing," Vacuum **63**, 385–431 (2001).
[9]D. Lundin, M. Stahl, H. Kersten, and U. Helmersson, "Energy flux measurements in high power impulse magnetron sputtering," J. Phys. D: Appl. Phys. **42**, 185202–185207 (2009).
[10]R. Piejak, V. Godyak, B. Alexandrovich, and N. Tishchenkoz, "Surface temperature and thermal balance of probes immersed in high density plasma," Plasma Sources Sci. Technol. **7**, 590–598 (1998).
[11]S. Bornholdt, M. Wolter, and H. Kersten, "Characterization of an atmospheric pressure plasma jet for surface modification and thin film deposition," Eur. Phys. J. D **60**, 653–660 (2010).
[12]R. Dussart, A. L. Thomann, L. E. Pichon, L. Bedra, N. Semmar, P. Lefaucheux, J. Mathias, and Y. Tessier, "Direct measurements of the energy flux due to chemical reactions at the surface of a silicon sample interacting with a SF6 plasma," Appl. Phys. Lett. **93**, 131502 (2008).
[13]M. Freed, M. V. P. Krüger, K. Poolla, and C. J. Spanos, "Wafer-grown heat flux sensor arrays for plasma etch processes," IEEE Trans. Semi. Manuf. **18**, 148 (2005).
[14]A. N. Magunov, "Scanning calorimetry measurements of the energy parameters of a plasmochemical polymer oxidation reaction," Plasma Phys. Rep. **28**, 359–366 (2002).
[15]A. Anders, "Atomic scale heating in cathodic arc plasma deposition," Appl. Phys. Lett. **80**, 1100 (2002).
[16]D. G. Cahill, K. Goodson, and A. Majumdar, "Thermometry and thermal transport in micro/nanoscale solid-state devices and structures," J. Heat Transfer **124**, 223–241 (2002).
[17]D. G. Cahill, W. K. Ford, K. E. Goodson, G. D. Mahan, A. Majumdar, H. J. Maris, R. Merlin, and S. R. Phillpot, "Nanoscale Thermal Transport," J. Appl. Phys. **93**, 793–818 (2003).
[18]D. G. Cahill, P. V. Braun, G. Chen, D. R. Clarke, S. Fan, K. E. Goodson, P. Keblinski, W. P. King, G. D. Mahan, A. Majumdar, H. J. Maris, S. R. Phillpot, E. Pop, and L. Shi, "Nanoscale thermal transport. II. 2003-2012," Appl. Phys. Rev. **1**, 011305 (2014).
[19]A. Giri, J. T. Gaskins, B. M. Foley, R. Cheaito, and P. E. Hopkins, "Experimental evidence of excited electron number density and temperature effects on electron-phonon coupling in gold films," J. Appl. Phys. **117**(4), 044305 (2015).
[20]X. Lu, M. Laroussi, and V. Puech, "On atmospheric-pressure non-equilibrium plasma jets and plasma bullets," Plasma Sources Sci. Technol. **21**, 034005 (2012).
[21]X. Lua, G. V. Naidis, M. Laroussi, and K. Ostrikov, "Guided ionization waves: Theory and experiments," Phys. Rep. **540**, 123–166 (2014).
[22]S. Hofmann, A. Sobota, and P. Bruggeman, "Transitions between and control of guided and branching streamers in dc nanosecond pulsed excited plasma jets," IEEE Trans. Plasma Sci. **40**, 2888–2899 (2012).
[23]J.-S. Oh, Y. Aranda-Gonzalvo, and J. W. Bradley, "Time-resolved mass spectroscopic studies of an atmospheric-pressure helium microplasma jet," J. Phys. D: Appl. Phys. **44**, 365202 (2011).
[24]T. B. Petrova, G. M. Petrov, D. R. Boris, and S. G. Walton, "Non-equilibrium steady-state kinetics of He-air atmospheric pressure plasmas," Phys. Plasmas **24**, 013501 (2017).
[25]A. Giri, J. T. Gaskins, B. F. Donovan, C. Szwejkowski, R. J. Warzoha, M. A. Rodriguez, J. Ihlefeld, and P. E. Hopkins, "Mechanisms of nonequilibrium electron-phonon coupling and thermal conductance at interfaces," J. Appl. Phys. **117**(10), 105105 (2015).
[26]P. E. Hopkins, L. M. Phinney, and J. R. Serrano, "Reexamining electron-Fermi relaxation in gold films with a nonlinear thermoreflectance model," J. Heat Transfer **133**, 044505 (2011).
[27]J. L. Braun and P. E. Hopkins, "Upper limit to the thermal penetration depth during modulated heating of multilayer thin films with pulsed and continuous wave lasers: A numerical study," J. Appl. Phys. **121**, 175107 (2017).
[28]J. L. Braun, C. J. Szwejkowski, A. Giri, and P. E. Hopkins, "On the steady-state temperature rise during laser heating of multilayer thin films in optical pump-probe techniques," J. Heat Transfer **140**(5), 052801 (2018).
[29]S. Große-Kreul, S. Hübner, S. Schneider, D. Ellerweg, A. von Keudell, S. Matejčík, and J. Benedikt, "Mass spectrometry of atmospheric pressure plasmas," Plasma Sources Sci. Technol. **24**, 044008 (2015).
[30]E. Stoffels, Y. Sakiyama, and D. B. Graves, "Cold atmospheric plasma: Charged species and their interactions with cells and tissues," IEEE Trans Plasma Sci. **36**, 1441 (2008).
[31]J. A. Rees, D. L. Seymour, C. L. Greenwood, Y. Aranda-Gonzalvo, and D. T. Lundie, "Mass and energy spectrometry of atmospheric pressure plasmas," Plasma Process. Polym. **7**, 92 (2010).
[32]K. McKay, J.-S. Oh, J. L. Walsh, and J. W. Bradley, "Mass spectrometric diagnosis of an atmospheric pressure helium microplasma jet," J. Phys. D: Appl. Phys. **46**, 464018 (2013).
[33]Y. Sakiyama, D. B. Graves, and E. Stoffels, "Influence of electrical properties of treated surface on RF-excited plasma needle at atmospheric pressure," J. Phys. D: Appl. Phys. **41**, 095204 (2008).
[34]H. F. Winters, H. Coufal, C. T. Rettner, and D. S. Bethune, "Energy transfer from rare gases to surfaces: Collisions with gold and platinum in the range 1—4000 ev," Phys. Rev. B **41**, 6240 (1990).
[35]M. Wolter, S. Bornholdt, M. Häckel, and H. Kersten, "Atmospheric pressure plasma jet for treatment of polymers," J. Achiev. Mater. Manuf. Eng. **37**, 730 (2009).
[36]M. Fröhlich, S. Bornholdt, C. Regula, J. Ihde, and H. Kersten, "Determination of the energy flux of a commercial atmospheric-

pressure plasma jet for different process gases and distances between nozzle outlet and substrate surface," Contrib. Plasma Phys. **54**, 155–161 (2014).
[37]T. Kewitz, M. Fröhlich, J. von Frieling, and H. Kersten, "Investigation of a commercial atmospheric pressure plasma jet by a newly designed calorimetric probe," IEEE Trans. Plasma Sci. **43**, 1769 (2015).
[38]F. Abeles, "Optics of thin films," in *Advanced Optical Techniques*, edited by A. C. S. V. Heel (North-Holland Publishing Co., Amsterdam, 1967), pp. 145–188.
[39]J. Hohlfeld, S. S. Wellershoff, J. Gudde, U. Conrad, V. Jahnke, and E. Matthias, "Electron and lattice dynamics following optical excitation of metals," Chem. Phys. **251**, 237–258 (2000).